coatings

MDPI

Article

Investigation of Silver Nanowire Transparent Heated Films Possessing the Application Scenarios for Electrothermal Ceramics

Yefu Hu and Weimin Wu *

International College, Krirk University, Bangkok 10220, Thailand; huyuehui@jci.edu.cn
* Correspondence: 2019008@cqust.edu.cn

Abstract: As transparent heated films (THFs) based on transparent conductive oxides (TCOs) are restricted by expensive raw materials and inappropriate fabricating film on curved surfaces because of its brittleness, silver nanowires transparent conductive film (AgWS-TCF) is an ideal alternative material for THF. However, there are still many problems to be solved in the electrical and thermal stability of AgNWs-TCF. In this paper, an Al-doped ZnO (AZO) nanoparticles produced by magnetron sputtering was used to modify and coat the AgNWs network, and the ceramic /AgNWs@AZO-TCF was obtained. Compared with ceramic/AgNWs-TCF, the sheet resistance of ceramic/AgNWs@AZO-TCF decreased from 53.2 to 19.3 Ω/sq, resistance non-uniformity decreased from 18.0% to 7.0%, and the inoxidizability, current-impact resistance, and failure voltage increased significantly. In addition, the electrothermal efficiency of ceramic/AgNWs@AZO-TCF is significantly improved after sputtering a SiO_2 layer on the surface of ceramic substrate. Compared with ceramic/AgNWs@AZO-TCF, the temperature of ceramic-SiO_2/AgNWs@AZO-TCF increases from 78.7 to 113.2 °C under applied voltage of 6 V, which possess the application scenarios for electrothermal-ceramics teacup (or tableware) to realize the function of heat preservation and disinfection.

Keywords: transparent film heaters; electrothermal stability; silver nanowires transparent conductive film; resistance non-uniformity; electrothermal ceramic

Citation: Hu, Y.; Wu, W. Investigation of Silver Nanowire Transparent Heated Films Possessing the Application Scenarios for Electrothermal Ceramics. *Coatings* **2023**, *13*, 607. https://doi.org/10.3390/coatings13030607

Academic Editor: Csaba Balázsi

Received: 15 February 2023
Revised: 8 March 2023
Accepted: 10 March 2023
Published: 13 March 2023

1. Introduction

Transparent heated film (THF) refers to visual transparency (both substrate and conductive film are transparent). When the current flows over a transparent conductive layer, it produces heat due to the Joule heating effect. This kind of heat can be used in the fields of smart windows, ice and haze removal, hot cushions, sensors, and other fields. Compared with traditional heating components, the THF has become one of the fastest growing markets at present due to its small thermal inertia.

The THF include the transparent conductive oxides (TCOs) [1–7], the carbon-based nanomaterials (carbon nanotubes and graphene), metal nano wires (MNWs) network [8–14], and conductive polymer materials [15]. Among them, one-dimensional silver nanostructural material has received widespread attention due to its excellent photoelectricity, thermal performance, and mechanical properties [10–14]. The silver nanowires (AgNWs) not only have many beneficial features of one-dimensional materials, but also inherit the high conductance (6.39 S/m) and excellent thermal conductivity of silver (429 W/(M·K)) [10]. AgNWs-TCF, a transparent conducting film fabricated from silver nanowires, has a unique advantage for transparent heater applications [16]. A good heater in commerce requires uniform heat distribution in the heating area, and usually achieves the target temperature at low voltage (<10V). Therefore, increasing the failure voltage of AgNWs-TCF, the lower limit of the working voltage, and the upper limit of the increase in temperature are the three working goals pursued by the AgNWs-based transparent heater [17]. But there are still many problems, among them, the electrical failure is one of the

bottlenecks that restrict the application of the AgNWs network to the large current transparent heater. This is because the method using AgNWs solution to fabricate the AgNWs-TCF by rotating coat and scratching coat has the following problems [18]. First, AgNW-TCFs have high junction resistance caused by nanowire-nanowire (NW-NW) junction in AgNW network and poor inoxidizability caused by high specific surface of AgNWs. Second, there exists thermal non-uniformity of AgNW-TCFs because of high junction resistance. If the hot spot does not spread rapidly along the conductive layer material or the substrate, it may cause local heating and become a local hot spot area. These hot spots may cause local degradation in the THFs area, which further exacerbates the non-uniformity of the conductive channel and causes further deterioration of electrical performance. Therefore, this is a problem that needs to be solved for the THFs of AgNWs-TCF. At present, the post-treatment methods of hot melt-weld and chemical modification were mainly used to reduce the junction resistance and increase the uniformity of heat distribution.

Annealing melt-weld, UV treatment, and water mist method are usually adopted [19] to perform post processing of AgNWs-TCF, which has achieved good results in reducing the NW-NW junction resistance of the AgNWs network. Nevertheless, these methods cannot solve the problem of electrical failure caused by the random distribution of silver nano wires that cause loading imbalance. For the problem of solving uneven heat distribution, the principle is that the conductive layer resistance of the silver nanowire network is evenly distributed by the appropriate process [19,20]. The NW–NW junction in nanowire network is tightly contacted by chemical modification (such as graphene sheet) to increase the ability of current-impact resistance and thermal migration [21,22], which improve significantly its electrical stability. The effective means to solve the thermal oxidation problem of the AgNWs network is isolating the water oxygen from the environment. Using a thin layer of oxide coating to improve inoxidizability of AgNWs in environment is one of the current effective means. The atmospheric pressure space atomic layer deposition (AP-SALD) technology to fabricate a ZnO film layer has greatly improved the electrical stability of THF in the environment [23].

The main performance parameters of the THF and its expected relation requirements may have different emphasis according to the different target application scenarios. In this paper, we propose using the Al-doped ZnO (AZO)-activated nanoparticles produced by magnetron sputtering to modify the NW–NW junction and wrap the AgNWs in order to obtain the THFs of AgNWs@AZO-TCF. This THFs possess low application voltage (<10 V), high electrothermal efficiency, and high stability (electrical performance stability, heat resistance, and inoxidizability), which can be applied to electrothermal ceramic teacups and electrothermal ceramic tile.

2. Materials and Methods

The silver nanowires (AgNWs, product number: 102886) colloid precursor was purchased from Jiangsu Xianfeng Nanomaterial Technology Corp. Ltd, Jiangsu, China. (Analytical Reagent, AR). The solution mainly includes isopropanol (IPA, AR), ethyl alcohol absolute (AR) which were obtained from Tianjin Yufutai Chemical Reagent Co., Ltd, Tianjin, China. The ethylene glycol is AR and obtained from Tianjin Hengmao Chemical Reagent Co., Ltd, Tianjin, China. The substrate (ceramic, glass, and ceramic-SiO_2), whose specification is summarized in Table S1 in Supplementary Materials, is cleaned by the semiconductor cleaning process and was placed on a spin coater (Institute of Electrics, Chinese Academy of Sciences, Beijing, China). The thin film preparation process was performed according to the technical route shown in Figure 1: the AgNWs solution was diluted by mixing 1.5 mL of silver nanowires and 4.5 mL of isopropanol. The diluted AgNWs solution was extracted with a plastic tip dropper and dropped on the substrate. After rotating at 600 rpm for 8 s first, the AgNWs wet film was obtained by rotating at 2000 rpm for 30 s. The AgNWs wet film was placed on a 100 °C heating-table for heat treatment for 5 min. The above process was repeated three times to obtain the ceramic/AgNWs-TCFs, glass/AgNWs-TCFs, and ceramic-SiO_2/AgNWs-TCFs samples, respectively. Al-doped ZnO (AZO) nanoparticles, produced

by magnetron sputtering method, were sputtered on the surfaces of ceramic/AgNWs-TCFs, glass/AgNWs-TCFs, and ceramic-SiO_2/AgNWs-TCFs samples respectively to wrap the silver nanowires and modify the AgNWs networks NW–NW junctions obtaining ceramic/AgNWs@AZO-TCFs, glass/AgNWs@AZO-TCFs, ceramic-SiO_2/AgNWs@AZO-TCFs shown in Figure 1d. The magnetron sputtering process was set as follows: working pressure of 1.2 Pa; power of 120 W; argon flow of 40 sccm for all samples; the sputtering time for the glass/AgNWs@AZO-TCFs and ceramic-SiO_2/AgNWs@AZO-TCFs was determined based on the optimal wrapping-layer effect of ceramic/AgNWs@AZO-TCFs, which was set as 0, 10, 20, 30, and 40 min, respectively, correspondingly remarked as samples 1#, 2#, 3#, 4#, and 5#.

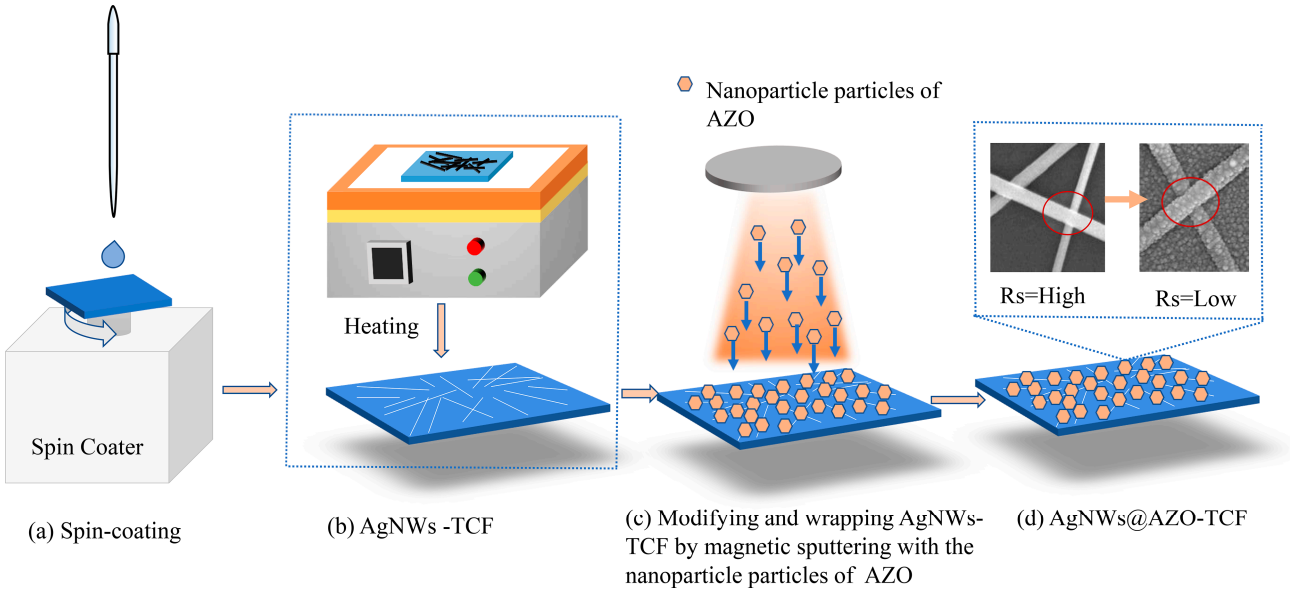

Figure 1. Schematic of AgNW network modification with AZO nanoparticles. (**a**) Spin-coating process in fabricating the wet AgNW TCFs. (**b**) The decolloid process of wet AgNW-TCFs by heating, (**c**) The modification process of AgNW network using AZO nanoparticles. (**d**) The NW–NW junction resistance of AgNW-TCFs (**left**) and AgNW@AZO-TCFs (**right**), *Rs* represents the sheet resistance of carrier transport across the NW–NW junction.

The surface morphology of the films was analyzed by JSM-6700F scanning electron microscope (JEOL Company, Tokyo, Japan). The roughness of surface was carried out on a Dimension Icon atomic force microscope (AFM, Dimension Icon, Bruker Company, Karisruhe, Germany), and set the signal of target tapping voltage of 5 V, cantilever frequency of 350 kHz, scanning rate of 0.2 Hz. The sheet resistance was measured using a resistance four-probe tester (KDY-1), the probe spacing is of 1 mm, and the current is set at 453.2 mA. At the same time, the thickness of the film should be less than 1 μm. Moreover, the withstand voltage of samples was tested using PRECI-200 series bench table source meter, and the temperature was measured using a Guide-P120V thermal imager. All operations and measurements are carried out at room temperature. A Beckman DU-8B ultraviolet–visible (UV–vis) spectrophotometer (Bankman-Du 8B Spectrophono-meter, Pullout General Instrument Company, Beijing, China) was used to measure the transmittance of the TCFs.

3. Results and Discussion

3.1. Superficial and Interfacial Properties

Figure 2 shows the surface and structural characteristics of AgNW-TCF modified by AZO nanoparticles. The silver nanowires network of samples before and after modification can be clearly detected in the figure, indicating that the AgNWs network is processed with AZO nanoparticles produced by magnetron sputtering to modify it rather than

forming a multilayer structure film. Figure 2a shows that the NW–NW junction contact of the unmodified sample 1# is not tight and poorly bonded to the substrate, and there is even a large gap between the silver nanowires network and the substrate, as shown in Figure 2a marked as A. As can be seen from Figure 2b–e, with the increase in sputtering time, the contact of NW–NW junction between AgNWs network and substrate becomes closer. However, it also can be seen from Figure 2(a1–e1) that the surface roughness of the sample decreases first and then increases with the increase in sputtering time. The surface roughness Ra of samples 1#, 2#, 3#, 4#, and 5# is summarized in Table S2 as shown in Supplementary Materials, which will affect the electrical properties of the conductive films if the degree of surface roughness is too high. The average AZO nano cluster size of samples 2#, 3#, 4#, and 5# was estimated to be of 12, 22, 45, and 60 nm, respectively.

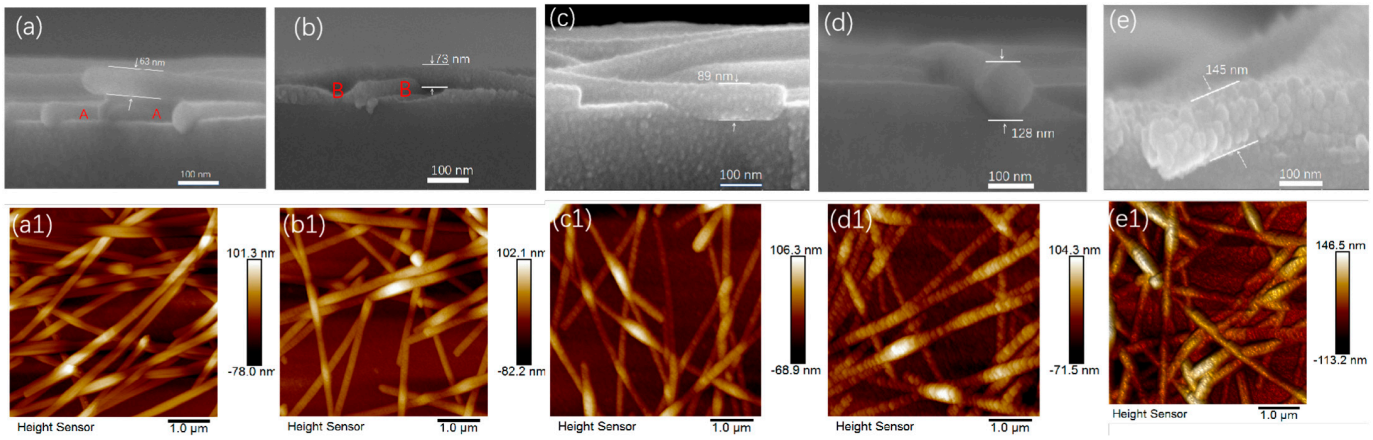

Figure 2. The images of surface topography for AgNWs-TCF and AgNWs@AZO-TCF. (**a**) The cross-sections SEM images of Ceramic/Agnws-TCF, and (**b–e**) ceramic/AgNWs@AZO-TCFs modified by AZO nanoparticles with 10, 20, 30, and 40 min, respectively. (**a1**) The 2D AFM image of ceramic/AgNWs-TCF, and (**b1–e1**) ceramic/AgNWs@AZO-TCFs modified by AZO nanoparticles with 10, 20, 30 and 40 min, respectively.

The UV–vis light-transparent spectrum shows in Figure 3 that the wavelength positions of the absorption peaks for samples 1#, 2#, 3#, 4#, and 5# are of 385, 392, 392, 393 and 396 nm, respectively, which exhibit an evident redshift for the ceramic/AgNWs@AZO-TCFs. This is because the AZO nanoparticles form a similar core (AgNWs)-shell (AZO nanoparticles) structure around the AgNWs conductive network. As seen in Figure 2a–e, the thicknesses of the wrapping-layer (shell layer) for samples 2#, 3#, 4#, and 5# are of 5, 13, 32, and 41 nm, respectively. An increase in the shell layer thickness enhances the pressure on the AgNWs, thereby changing the contraction effect of the AgNWs lattice, showing a trend that the thicker the shell layer, the more significant the redshift will be [24].

In summary, using the AZO nanoparticles produced by magnetron sputtering in AgNWs conductive network can modify the NW–NW junction and wrap the AgNWs, which is important to improve the electrical properties and stability properties. Sputtering time plays an important role in surface roughness and wrapping-layer thickness. Sample 3# with sputtering time of 20 min shows the best comprehensive effect of surface roughness and wrapping-layer thickness.

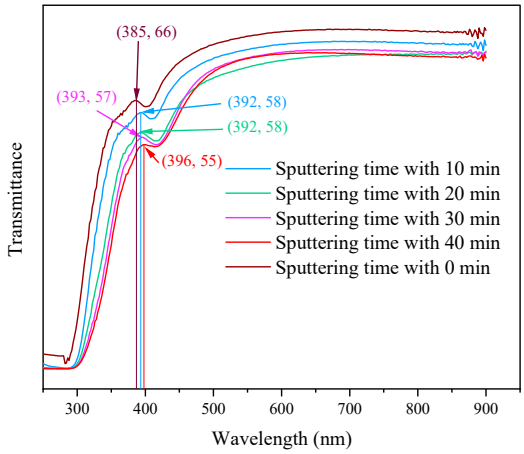

Figure 3. UV-vis light transparent spectra of ceramic /AgNW @ AZO-TCF after different sputtering times.

3.2. Electrical Property

The sheet resistances have been tested at 25 positions for samples 1#~5#, with the results shown in Figure 4. The average resistance, decrease rate of resistance, non-uniformity of resistance distribution are summarized in Table 1. It was found that the longer the sputtering time, the more obvious the sample resistance reduction. However, compared with sample 3#, the resistance values of the samples 4# and 5# were increased after the sputtering time was too long. The resistance of ceramic/AgNWs@AZO-TCFs has a close relationship with the effect of AZO nanoparticles modification, involving the contact tightness and surface roughness of NW–NW junctions of silver nanowires.

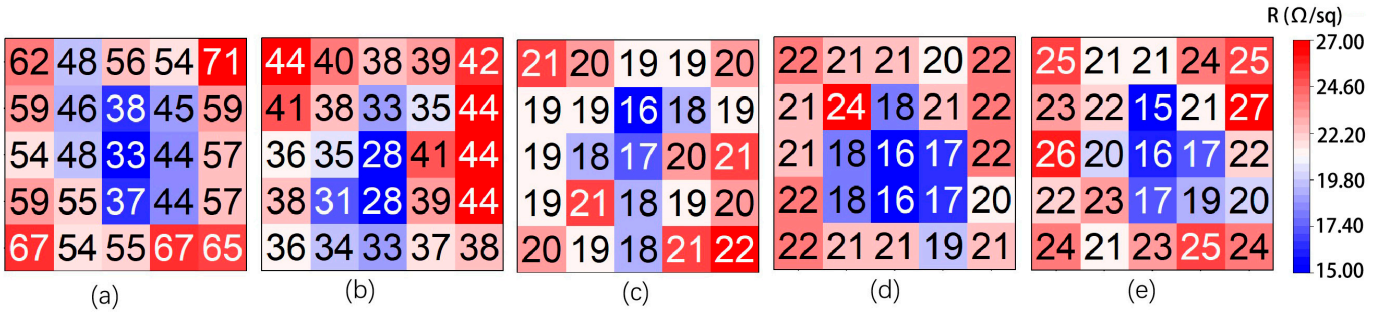

Figure 4. Distribution of sheet resistance. (**a**) Distribution of sheet resistance for the ceramic/AgNWs-TCF; (**b**–**e**) Distribution of sheet resistance for the ceramic/ AgNWs@AZO-TCFs modified by AZO nanoparticles with 10, 20, 30, and 40 min, respectively.

Table 1. Electrical properties change of ceramic/AgNWs@AZO-TCFsVs sputtering time.

Sample	1#	2#	3#	4#	5#
Sputtering time (min)	-	10	20	30	40
Average Resistance (Ω/sq)	53.2	37.4	19.3	20.1	21.7
NUF * (%)	18.0	12.1	7.0	10.4	14.1
Reduction rate of resistance (%)	-	29.7	63.7	62.2	59.2

* NUF represents non-uniformity degrees.

Compared with reference sample 1#, what improved the conductivity performance of AgNWs@AZO-TCF should be attributed to the results of AZO nanoparticles modified

and wrapped in AgNWs network. In AgNWs-TCF, the NW-NW junction in AgNWs network contacts loosely as showing Figure 2a,a1, resulting in high junction resistance. For AgNWs@AZO-TCF, the AZO nanoparticles produced by magnetron sputtering bombard the AgNWs network, at the same time; the AgNWs shows similar core-shell structure, and the NW–NW junction is modified to make NW–NW junction and AgNWs-substrate tight. As a result, the resistance of AgNWs@AZO-TCF was reduced. For sample 2#, the silver nanowires network can be modified poorly because of the AZO nanoparticles dealing with short sputtering time. It possess wrapping-layer thickness of only 5 nm, larger surface roughness Ra of 20.5 nm and poorer binding with substrate, seeing the mark B from in Figure 2b, which results in its conductivity worse than that of 3#~5#; although its conductivity is better than that of sample 1#. Sample 3# has the lowest resistance, which benefits from its appropriate wrapping-layer thickness of 13 nm, the lowest surface roughness Ra of 18.7 nm, and good binding degree with substrate when the sputtering time is 20 min, as shown in Figure 2c. However, the conductivities of sample 4# with Ra of 21.4 nm and sample 5# with Ra of 29.9 nm are worse than that of sample 3#, because their surface roughness is higher than that of sample 3#. Therefore, the conductivity of AgNWs@AZO-TCFs depends on the contact tightness and surface roughness of NW–NW junction of silver nanowires network.

According to Yonggao Jia et al. [25], non-uniformity is defined with the relative standard deviation as:

$$NUF = \sqrt{\frac{1}{n}\frac{\sum_{i=1}^{n}\left(R_i - \overline{R}\right)^2}{\overline{R}^2}} \quad (1)$$

where n is the number of measurements on the film of different sites, and R_i and $\overline{R}$ are the measured sheet resistance and the average resistance of all the measurements, respectively. Using the Equation (1), non-uniformity of samples 1#~5# was obtained as 18.0%, 12.1%, 7.0%, 10.4%, and 14.1%, respectively, indicating that the distribution uniformity of resistance is obviously improved after modified by AZO nano particles. It can be seen that appropriate wrapping-layer thickness is of great significance to improve the uniformity of electrical properties. Sample 3# which possesses wrapping-layer thickness of 13 nm has the best uniformity of electrical properties, followed by sample 4# with wrapping-layer thickness of 32 nm, sample 2# with wrapping-layer thickness of 5 nm, and sample 5# with wrapping-layer thickness of 41 nm; their non-uniformity of sheet resistance is 10.4%, 12.1%, and 14.1%, respectively. The possible reasons for the influence of wrapping-layer thickness on the uniformity of electrical properties are as follows: On the one hand, that high-energy AZO nanoparticles bombard the silver nanowires network makes the loose contact of NW-NW junction become flatter and more compact with the increase in sputtering time, which results in uniform transfer ability of carriers on the surface of the film under small surface roughness. On the other hand, for the limitation of diffusion energy, AZO nanoparticles coated on the surface of silver nanowires will accumulate due to the excessively long sputtering time. With the increase in sputtering time, the accumulation clusters will become larger and larger, for example, the size of the accumulation clusters of sample 5# is as large as 60 nm, as a result it makes the transport capacity of carriers on the surface of the film become uneven.

Table 2 and Figure 5a shows that the resistance of increasing rate for samples 1#, 2#, 3#, 4# and 5# is 135.3%, 36.6%, 8.8, 6.9, and 4.6% after exposing to air of 16 days, respectively, which indicate that the inoxidizability of AgNWs@AZO-TCF is significantly improved with the increase in wrapping-layer thickness. It can also be seen from Figure 5c that the failure voltages of samples 1#~5# are 8, 12, 14, 15, and 17 V respectively, indicating that the failure voltages of AgNWs@AZO-TCF improved with the increase in wrapping-layer thickness. The reason is that the silver nanowires network after modified by AZO nanoparticles forms a similar core-shell structure, which is beneficial to the improvement of inoxidizability performance and failure voltage for the AgNWs@AZO-TCF. Figure 5b shows the current-impact resistance of AgNWs-TCF and AgNWs@AZO-TCF samples. As can be seen from

Figure 5b that the conductivity of AgNWs-TCF fails after 6 h of continuous conduction when supplied with a voltage of 4V. For the AgNWs@AZO-TCFs, including samples 2#~5#, the conductivity still remains stable after 24 h of continuous conduction when supplied with a voltage of 4V, which indicates that its performance of current-impact resistance is obviously improved. This performance improvement of current-impact resistance for the AgNWs@AZO-TCFs should be attributed to the results of AZO nanoparticles modifying and wrapping in AgNWs network, which makes the NW–NW junction contact tightly and the AgNWs network becoming flat, consequently, having improved the migration capacity of current for the conductive channel in AgNWs network.

Table 2. Change of resistance in relation to exposing time in air.

Time (day)	0	2	4	6	8	10	12	14	16
$R_{1\#}$ (Ω/sq.)	53.2	53.8	54.5	59	63	71	80	100	125.2
$R_{2\#}$ (Ω/sq.)	37.4	37.8	38.0	39.1	41.0	43.9	46.2	49.3	51.1
$R_{3\#}$ (Ω/sq.)	19.3	19.3	19.3	19.5	20.0	20.1	20.2	20.4	21.0
$R_{4\#}$ (Ω/sq.)	20.1	20.1	20.1	20.3	20.6	20.7	20.9	21.0	21.5
$R_{5\#}$ (Ω/sq.)	21.7	21.7	21.7	21.7	21.9	22	22.3	22.5	22.7

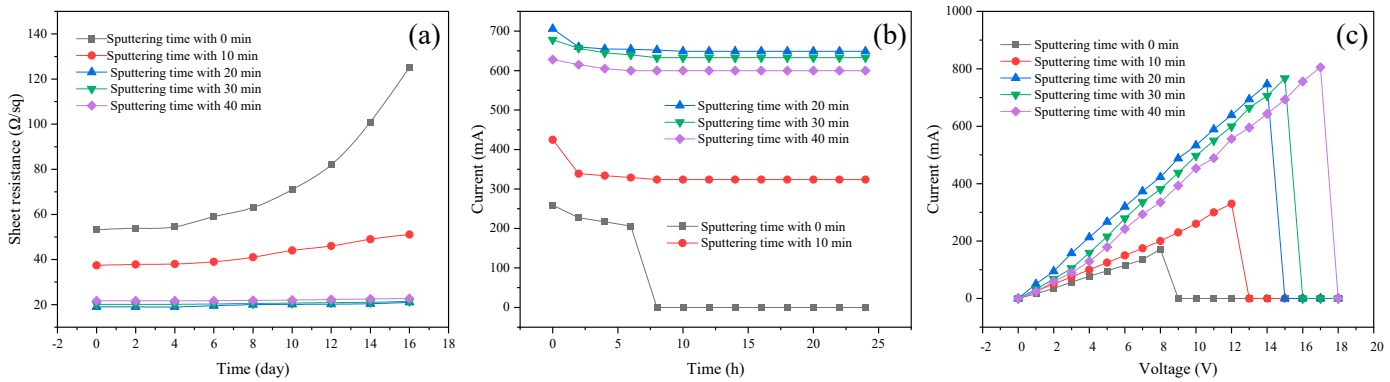

Figure 5. Electrical stability of AgNWs-TCF and AgNWs@AZO-TCF samples. (**a**) Performance of inoxidizability; (**b**) Performance of current–impact resistance; (**c**) Failure voltage.

In a word, the performance improvement of AgNWs@AZO-TCF, including the sheet resistance reduction, the resistance uniformity, the inoxidizability, current-impact resistance and stability (failure voltages), should be attributed to the results of AZO nanoparticles modified and wrapped in AgNWs network. In AgNWs-TCF, the NW–NW junction in AgNWs network contact loosely, resulting in high junction resistance. But for the AgNWs@AZO-TCF, the AZO nano particles bombard the AgNWs network, at the same time, the AgNWs is wrapped and formed core-shell structure, and the NW–NW junction is modified to make NW-NW junction and AgNWs-substrate tightly. As a result, the resistance of AgNWs@AZO-TCF was reduced, the distributed resistance becomes uniform, and the stability (inoxidizability, current-impact resistance, failure voltages) improved.

3.3. Thermal Properties

Figure 6a shows the performance of heating-resistance Vs wrapping-layer thickness. It can be seen that the higher the thickness of the wrapping-layer, the better the heating-resistance of the samples. In AgNWs-TCF, its heating-resistance temperature is 150 °C indicating the worst heating-resistance performance. But for the AgNWs@AZO-TCFs (samples 2#~5#), their heating-resistance temperatures are above 300 °C, which increase with thickness. The improvement in heating-resistance performance for AgNWs@AZO-TCFs should be attributed to the core-shell structure because the layer of AZO shell possesses the ability to resist thermal shock. Interestingly, Figure 6b shows the resistance decreases as

the temperature increases in the range from 100 to 250 °C, which should be attributed to the annealing melt-weld [19] in lower range of temperature.

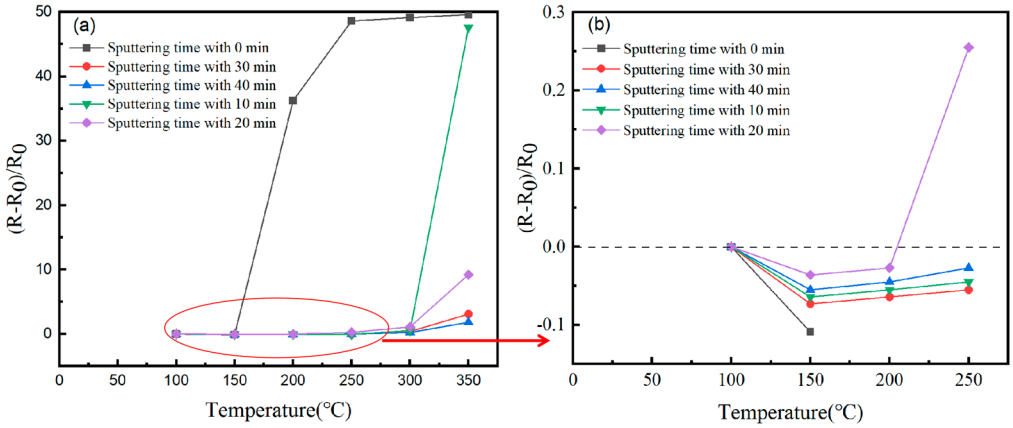

Figure 6. Performance of heating–resistance Vs wrapping–layer thickness. (**a**) Temperature region from 100 °C to 350 °C; (**b**) Temperature region from 100 to 250 °C.

Figure 7a shows the electrothermal efficiency of Ceramic/AgNWs-TCF and Ceramic/AgNWs@AZO-TCFs (samples 2#~5#), heating zone of all samples is 2.5 cm × 2.5 cm. As can be seen from the figure, the electrothermal efficiency of Ceramic/AgNWs@AZO-TCFs is obviously higher than that of Ceramic/AgNWs-TCF, of which 3# has the highest electrothermal efficiency, followed by samples 4#, 5#, 2# and 1# successively. The improvement in electrothermal efficiency for AgNWs@AZO-TCFs should be attributed to the resistance reduction after the silver nanowire network is modified by AZO nanoparticles. As previously discussed, the sheet resistance of AgNWs@AZO-TCFs modified by AZO nanoparticles produced by magnetron sputtering, has reduced. As showing in Table 2, the sheet resistance of samples 3#, 4#, 5#, 2# and 1# are 19.3, 20.1, 21.7, 37.4, and 53.2 Ω/sq, respectively. According to the Joule-heat formula of $P = V^2/R$, the smaller the resistance, the higher the electrothermal efficiency.

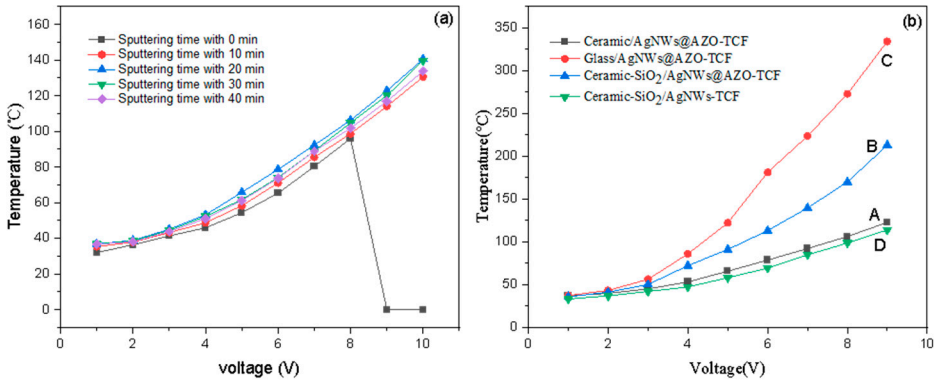

Figure 7. Electrothermal efficiency of AgNWs-TCF and AgNWs@AZO-TCFs. (**a**) Transparent heating film of ceramic substrate. (**b**) Transparent heating film of ceramic substrate, glass substrate, and ceramic-SiO_2 substrate, all samples with sputtering time of 20 min except Ceramic-SiO_2/AgNWs-TCF. The curves A, B, C and D represent ceramic/AgNWs@AZO-TCF, ceramic-SiO_2/AgNWs@AZO-TCF, glass/AgNWs@AZO-TCF and ceramic-SiO_2/AgNWs@-TCF respectively.

Figure 7b shows the electrothermal efficiency of transparent heating films on different substrates; the heating zone of all samples is 2.5 cm × 2.5 cm. The curve C in the Figure 7b is the glass/AgNWs@AZO-TCF (glass substrate). It can be seen that its electrothermal efficiency is much better than that of ceramic/AgNWs@AZO-TCF (ceramic substrate,

sample 3#). Considering that it may relates to the density and roughness of the substrate, the ceramic substrate was treated by sputtering a layer of SiO_2 film with a thickness of 0.5 μm on the ceramic substrate to obtain the ceramic-SiO_2 substrate, and the ceramic-SiO_2/AgNWs-TCF and ceramic-SiO_2/AgNWs@AZO-TCF samples were prepared on its surface. The curve B in Figure 7b shows that the electrothermal efficiency of ceramic-SiO_2/AgNWs@AZO-TCF is significantly higher than that of ceramic/AgNWs@AZO-TCF (sample 3#). Interestingly, comparing with ceramic/AgNWs-TCF shown in Figure 6a, the curve D in Figure 7 show that the failure voltage of ceramic-SiO_2/AgNWs-TCF improved, although its electrothermal efficiency is lower than ceramic/AgNWs@AZO-TCF. The reason why the ceramic-SiO_2 substrate can improve the electrothermal efficiency of THFs is that the density and flatness of the ceramic substrate are improved after sputtering a layer of SiO_2 on the ceramic substrate surface. Figure 8 shows the 2D AFM images of ceramic (glazed) substrate in Figure 8a; ceramic/SiO_2 substrate in Figure 8b; and glass substrate in Figure 8c, respectively. As can be seen from Figure 8c that the glass substrate has a high density with roughness *Ra* of 1.65 nm as shown in Supplementary Materials Table S2, much lower than that of the ceramic substrate with roughness *Ra* of 8.29 nm as shown in Supplementary Materials Table S2, and that of ceramic-SiO_2 substrate with roughness *Ra* of 4.20 nm as shown in Supplementary Materials Table S2. This low surface roughness of substrate is beneficial to heat reflection to THFs surface, as a result improving its electrothermal efficiency.

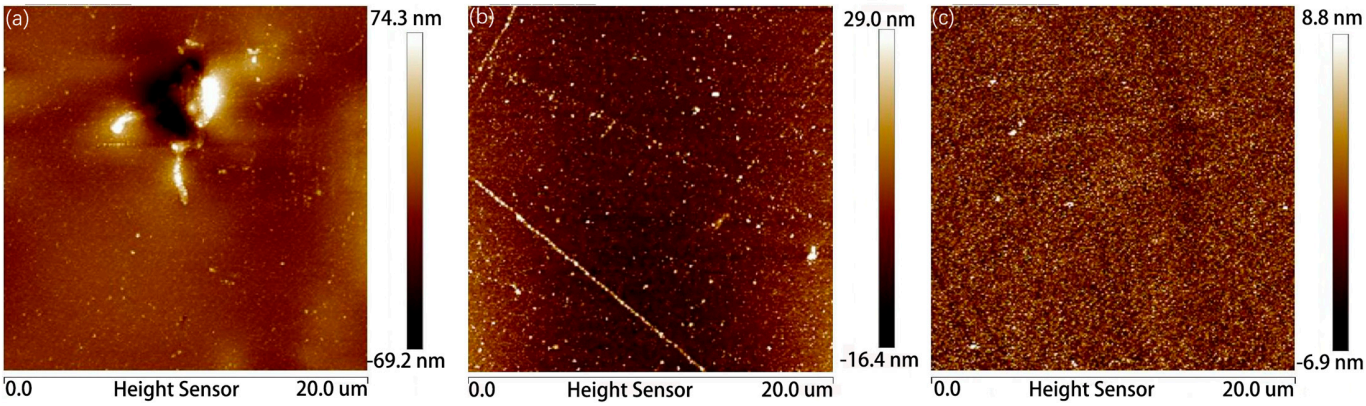

Figure 8. The 2D AFM images. (**a**) Ceramic substrate; (**b**) ceramic-SiO_2 substrate, and (**c**) glass substrate.

In a word, the electrothermal efficiency of THFs depends not only on its low resistance value, but also on the low surface roughness of the substrate. The ceramic-SiO_2/AgNWs@AZO-TCF obtained by sputtering a SiO_2 layer on the ceramic substrate surface and modifying the silver nanowire network with AZO nanoparticles has a good electrothermal efficiency, which shows that its surface temperature reaches 50.2, 72.3, 91.2, 113.2, and 213.1 °C at an applied voltage of 3, 4, 5, 6 and 9 V as shown in Figure 7b in the curve B, respectively. This means that the ceramic-SiO_2/AgNWs@AZO-TCF has a good electrothermal effect even at low voltage. The temperature of ceramic-SiO_2/AgNWs@AZO-TCF reaches 72.3 °C at an applied voltage of 4V, realized as the heat preservation functions if applied to ceramic devices such as electrothermal teacup, electrothermal tableware, and heating face (floor) tile. Furthermore, the temperature of ceramic-SiO_2/AgNWs@AZO-TCF reaches 113.2 °C at an applied voltage of 9 V, realized as the sterilization and disinfection function if applied to electrothermal teacup and electrothermal tableware.

Figure 9 shows the temperature distribution of ceramic/AgNWs-TCF and ceramic/AgNWs@AZO-TCFs (samples 2#~5#), in which different colors are used to represent different temperatures. As can be seen from the figures, the temperature distribution of sample 3# is the best uniform temperature, followed by samples 4#, 2#, 5#, and 1#, successively. Jeung Choon Goak et al. [26] have reported the non-uniformity of temperature

distribution for THFs using CCD thermoreflectance optical microscopy image coming from the non-uniformity of junction-resistance distribution. The reasons are explained as follows: According to the transient self-heating model of Sajia Sadeque et al. [27], the complex and random AgNW network is partially reduced to two geometrically symmetrical nanowires that intersect on the substrate in which a hot spot is formed at the junction and local thermoelectricity is generated. At the NW–NW junction, heat from the top flows to the upper nanowires and heat from the bottom flows to the down nanowires. For ceramic/AgNWs-TCF, because the contact area between the top silver nanowires and the bottom silver nanowires as well as between the bottom silver nanowires and the substrate is small due to the weak NW–NW junction contact and the weak contact between the bottom silver nanowires and the substrate as showing in Figure 2a,a1, the heat transfer is unbalanced, which results in the worst temperatures distribution of the ceramic/AgNWs-TCF. On the contrary, for ceramic/AgNWs@AZO-TCFs (samples 2#~5#), because the contact area between the top silver nanowires and the bottom silver nanowires as well as between the bottom silver nanowires and the substrate is large due to the tight NW–NW junction contact and the tight contact between the bottom silver nanowires and the substrate, as shown in Figure 2b–e, the heat transfer becomes balance, resulting in even surface temperatures of the ceramic/AgNWs@AZO-TCFs, in which the temperature distribution of sample 3# is the best uniform temperature, followed by samples 4#, 2#, 5#, and 1# successively, which is consistent with the uniformity of resistance distribution as shown in Table 1.

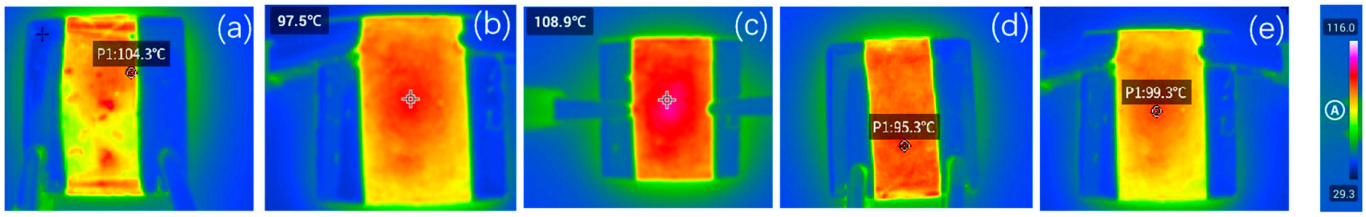

Figure 9. The thermal images of temperature distribution. (**a**) Ceramic/AgNWs-TCF; (**b**–**e**) ceramic/AgNWs@AZO-TCFs modified by AZO nanoparticles with 10, 20, 30, and 40 min, respectively.

4. Conclusions

AgNWs network was modified and wrapped by AZO nanoparticles produced by magnetron sputtering to form a core-shell structure, which, on the one hand, can make NW–NW junction contact tightly in AgNWs network greatly reducing the resistance of the junction and improving the electrical stability and heating efficiency of the AgNW-based heaters. On the other hand, the AZO coating can improve the inoxidizability and heat resistance of silver nanowire-based THF. Sputtering a layer of SiO_2 on the surface of the ceramic substrate effectively improves the surface thermal radiation of ceramic-SiO_2/AgNWs@AZO-TCF due to the smooth surface of SiO_2-ceramic. Therefore, the ceramic-SiO_2/AgNWs@AZO-TCF can be applied to the scenario of electrically heated ceramics that perform the functions of heat preservation and disinfection at low voltage, such as electrothermal teacup and electrothermal tableware. The uniformity of surface temperature for the silver nanowire-based THF depends on the tightness of NW–NW junction contact in AgNWs network and the closeness of AgNWs network to the substrate. AgNWs network can be modified and wrapped by AZO nanoparticles produced by magnetron sputtering, which can effectively improve the electrothermal uniformity of silver nanowire-based THF due to the tight NW–NW junction contact and the tight contact between the AgNWs network and the substrate.

Supplementary Materials: The following supporting information can be downloaded at: https://www.mdpi.com/article/10.3390/coatings13030607/s1. Table S1: Substrates specification: The details of area and specification for ceramic, glass, and ceramic-SiO_2 substrates. Table S2: Surface roughness *Ra* of transparent heating film and substrates: The surface roughness *Ra* of transparent heating films with sputtering time 0, 10, 20, 30, and 40 min is 20.2, 20.5, 18.7, 21.4, and 29.9 nm, respectively, and surface roughness *Ra* of ceramic, glass, and ceramic-SiO_2 substrates is 8.29, 1.65 and 4.20 nm, respectively.

Author Contributions: Conceptualization, Y.H.; methodology, Y.H.; software, Y.H.; formal analysis, W.W.; investigation, Y.H.; resources, Y.H. and W.W.; data curation, Y.H.; writing—original draft preparation, Y.H.; writing—review and editing, Y.H. and W.W.; supervision, W.W.; project administration, Y.H.; funding acquisition, Y.H. All authors have read and agreed to the published version of the manuscript.

Funding: This research was funded by the National Natural Science Foundation of China, grant numbers 62041405; the Natural Science Foundation of Jiangxi Province, China, grant numbers 20202BAB202011, 20202BABL214011; the Education Bureau of Jiangxi Province, China, grant numbers GJJ2201003, GJJ211328, GJJ211319; the Key R & D Program of Jiangxi Province, China, grant numbers 20192BBE50056 and 20171BBE50053; the National Ceramic Industry Design Institute of China, grant numbers NICID2022Z01.

Institutional Review Board Statement: Not applicable.

Informed Consent Statement: Not applicable.

Data Availability Statement: The data presented in this study are available on request from the corresponding author.

Acknowledgments: The authors thank the technical support from the School of Mechanical and Electrical Engineering, Jingdezhen Ceramic University. Thanks are extended to Hu Yuehui, Chen Yichuan, Liu Wei Min Zhi Jian, Dai Yanjie, and Zhou Ke, for technical assistance in measurement, and samples preparation, respectively.

Conflicts of Interest: The authors declare no conflict of interest.

References

1. Morales-Masis, M.; De Wolf, S.; Woods-Robinson, R.; Ager, J.W.; Ballif, C. Transparent Electrodes for Efficient Optoelectronics. *Adv. Electron. Mater.* **2017**, *3*, 1600529. [CrossRef]
2. Rey, G.; Ternon, C.; Modreanu, M.; Mescot, X.; Consonni, V.; Bellet, D. Electron Scattering Mechanisms in Fluorine-Doped SnO_2 Thin Films. *J. Appl. Phys.* **2013**, *114*, 183713. [CrossRef]
3. Nguyen, V.H.; Gottlieb, U.; Valla, A.; Muñoz, D.; Bellet, D.; Muñoz-Rojas, D. Electron Tunneling through Grain Boundaries in Transparent Conductive Oxides and Implications for Electrical Conductivity: The Case of ZnO:Al Thin Films. *Mater. Horiz.* **2018**, *5*, 715–726. [CrossRef]
4. Hecht, D.S.; Hu, L.; Irvin, G. Emerging Transparent Electrodes Based on Thin Films of Carbon Nanotubes, Graphene, and Metallic Nanostructures. *Adv. Mater.* **2011**, *23*, 1482–1513. [CrossRef]
5. Kim, B.-J.; Park, J.-S.; Yoo, R.; Park, J.-S. Flexible Grid-mesh Electrodes Fabricated by Electroless Copper Plating on Corona-treated PET Substrates and Coating with Graphene for Transparent Film Heaters. *RSC Adv.* **2017**, *7*, 53025–53031. [CrossRef]
6. Khan, A.; Liang, C.; Huang, Y.-T.; Zhang, C.; Cai, J.; Feng, S.-P.; Li, W.-D. Template-Electrodeposited and Imprint-Transferred Microscale Metal-Mesh Transparent Electrodes for Flexible and Stretchable Electronics. *Adv. Eng. Mater.* **2019**, *21*, 1900723. [CrossRef]
7. Thouti, E.; Mistry, C.; Chandran, A.; Kumar Panwar, D.; Kumar, P.; Suman, H.; Akhtar, J. Study of Seamless Au Mesh Flexible Transparent Heaters: Influence of Mesh Coverage. *J. Phys. D: Appl. Phys.* **2019**, *52*, 425301. [CrossRef]
8. Li, L.; Yu, Z.; Hu, W.; Chang, C.-H.; Chen, Q.; Pei, Q. Efficient Flexible Phosphorescent Polymer Light-Emitting Diodes Based on Silver Nanowire-Polymer Composite Electrode. *Adv. Mater.* **2011**, *23*, 5563–5567. [CrossRef]
9. Zhao, S.; Han, F.; Li, J.; Meng, X.Y.; Huang, W.P.; Cao, D.X.; Zhang, G.P.; Sun, R.; Wong, C.P. Advancements in Copper Nanowires: Synthesis, Purification, Assemblies, Surface Modification, and Applications. *Small* **2018**, *14*, 1800047. [CrossRef]
10. Tan, D.; Jiang, C.; Li, Q.; Bi, S.; Song, J. Silver Nanowire Networks with Preparations and Applications: A Review. *J. Mater. Sci. Mater. Electron.* **2020**, *31*, 15669–15696. [CrossRef]
11. Kwon, J.; Suh, Y.D.; Lee, J.; Lee, P.; Han, S.; Hong, S.; Yeo, J.; Lee, H.; Ko, S.H. Recent Progress in Silver Nanowire based Flexible/Wearable Optoelectronics. *J. Mater. Chem. C* **2018**, *6*, 7445–7461. [CrossRef]
12. Sun, Y.; Chang, M.; Meng, L.; Wan, X.; Gao, H.; Zhang, Y.; Zhao, K.; Sun, Z.; Li, C.; Liu, S.; et al. Flexible Organic Photovoltaics based on Water-Processed Silver Nanowire Electrodes. *Nat. Electron.* **2019**, *2*, 513–520. [CrossRef]

13. Li, W.; Zhang, H.; Shi, S.; Xu, J.; Qin, X.; He, Q.; Yang, K.; Dai, W.; Liu, G.; Zhou, Q.; et al. Recent Progress in Silver Nanowire Networks for Flexible Organic Electronics. *J. Mater. Chem. C* **2020**, *8*, 4636–4674. [CrossRef]
14. Liu, W.; Hu, Y.; Chen, Y.; Hu, Z.; Zhou, K.; Min, Z.; Liu, H.; Zhan, L.; Dai, Y. Improvement of Electrical Properties of Silver Nanowires Transparent Conductive by Metal Oxide Nanoparticles Modification. *Coatings* **2022**, *12*, 1816. [CrossRef]
15. Gueye, M.N.; Carella, A.; Demadrille, R.; Simonato, J.-P. All-Polymeric Flexible Transparent Heaters. *ACS Appl. Mater. Interfaces* **2017**, *9*, 27250–27256. [CrossRef] [PubMed]
16. Kim, T.; Kim, Y.W.; Lee, H.S.; Kim, H.; Yang, W.S.; Suh, K.S. Uniformly Interconnected Silver-Nanowire Networks for Transparent Film Heaters. *Adv. Funct. Mater.* **2013**, *23*, 1250–1255. [CrossRef]
17. Zhu, Y.; Deng, Y.; Yi, P.; Peng, L.; Lai, X.; Lin, Z. Flexible Transparent Electrodes Based on Silver Nanowires: Material Synthesis, Fabrication, Performance, and Applications. *Adv. Mater. Technol.* **2019**, *4*, 1900413. [CrossRef]
18. Hwang, B.-Y.; Choi, S.-H.; Lee, K.-W.; Kim, J.-Y. Highly Stretchable and Transparent Electrode Film based on SWCNT/Silver Nanowire Hybrid Nanocomposite. *Compos. Part B Eng.* **2018**, *151*, 1–7. [CrossRef]
19. Hu, Y.; Hu, F.; Chen, Y.; Gao, H.; Liu, W.; Zhou, K.; Min, Z.; Zhu, W. Shear Force Strategy for Preparation of Aligned Silver Nanowire Transparent Conductive Thin Films. *Colloid Interface Sci. Commun.* **2023**, *52*, 100685. [CrossRef]
20. Ke, S.; Xie, J.; Chen, C.; Lin, P.; Wang, D. Van der Waals Epitaxy of Al-Doped ZnO Film on Mica as a Flexible Transparent Heater with Ultrafast Thermal Response. *Appl. Phys. Lett.* **2018**, *112*, 031905. [CrossRef]
21. Cao, M.; Wang, M.; Li, L.; Qiu, H.; Yang, Z. Effect of Graphene-EC on Ag NW-Based Transparent Film Heaters: Optimizing the Stability and Heat Dispersion of Films. *ACS Appl. Mater. Interfaces* **2018**, *10*, 1077–1083. [CrossRef]
22. Cai, Y.; Piao, X.; Yao, X.; Gao, W.; Nie, E.; Zhang, Z.; Sun, Z. Transparent Conductive Film based on Silver Nanowires and Single-Wall Carbon Nanotubes for Transparent Heating Films. *Nanotechnology* **2019**, *30*, 225201. [CrossRef] [PubMed]
23. Khan, A.; Nguyen, V.H.; Muñoz-Rojas, D.; Aghazadehchors, S.; Jiménez, C.; Nguyen, N.D.; Bellet, D. Stability Enhancement of Silver Nanowire Networks with Conformal ZnO Coatings Deposited by Atmospheric Pressure Spatial Atomic Layer Deposition. *ACS Appl. Mater. Interfaces* **2018**, *10*, 19208–19217. [CrossRef] [PubMed]
24. Bothwell, T.; Kennedy, C.J.; Aeppli, A.; Kedar, D.; Robinson, J.M.; Oelker, E.; Staron, A.; Ye, J. Resolving the Gravitational Redshift across a Millimetre-Scale Atomic Sample. *Nature* **2022**, *602*, 420–424. [CrossRef]
25. Jia, Y.; Chen, C.; Jia, D.; Li, S.; Ji, S.; Ye, C. Silver Nanowire Transparent Conductive Films with High Uniformity Fabricated via a Dynamic Heating Method. *ACS Appl. Mater. Interfaces* **2016**, *8*, 9865–9871. [CrossRef]
26. Goak, J.C.; Kim, T.Y.; Kim, D.U.; Chang, K.S.; Lee, C.S.; Lee, N. Stable Heating Performance of Carbon Nanotube/silver Nanowire Transparent Heaters. *Appl. Surf. Sci.* **2020**, *510*, 145445. [CrossRef]
27. Sadeque, S.; Candadai, A.; Gong, Y.; Maize, K.; Ziabari, A.K.; Mohammed, A.M.S.; Shakouri, A.; Fisher, T.; Janes, D.B. Transient Self-Heating at Nanowire Junctions in Silver Nanowire Network Conductors. *IEEE Trans. Nanotechnol.* **2018**, *17*, 1171–1180. [CrossRef]